Hindawi
Journal of Spectroscopy
Volume 2019, Article ID 5395914, 10 pages
https://doi.org/10.1155/2019/5395914

Research Article

Effects of Working Medium Gases on Emission Spectral and Temperature Characteristics of a Plasma Igniter

Gao Cheng Chen,[1,2] **Li Ming He**,[2] **Bing Bing Zhao**,[2] **Hua Lei Zhang**,[3] **Zi Chen Zhao**,[1,2] **Hao Zeng**,[2] **Jian Ping Lei**,[1,2] **and Xiong Liu**[1,2]

[1]*Graduate School, Air Force Engineering University, Xi'an 710051, China*
[2]*Aeronautic Engineering College, Air Force Engineering University, Xi'an 710038, China*
[3]*Institute of Aviation Operation Service, Aviation University of Air Force, Changchun 13022, China*

Correspondence should be addressed to Bing Bing Zhao; zhaobingbing_afeu@163.com

Received 28 April 2019; Accepted 19 July 2019; Published 29 August 2019

Academic Editor: Jeongkwon Kim

Ar, N_2, O_2, and N_2-O_2 mixture under different O_2 components were separately used as the working medium gas of a plasma igniter to study the influence of working-medium-gas type and O_2 concentration on emission spectral and temperature characteristics of a direct-current arc plasma igniter. The emission spectra of the plasma jet were also analyzed using the optical emission spectroscopy method, and the influence rule of working medium gas and O_2 concentration on electron temperature and vibrational temperature of the plasma jet was calculated and analyzed. The experimental results show that the emission spectra of the plasma jet had significant differences when diverse working gases were used as the working medium of the igniter. With increasing O_2 concentration in the working medium gas, the spectral line intensity of oxygen-containing particles in emission spectra of the plasma jet was significantly enhanced, and the spectral intensities of nitrogen-containing particles, NO molecular bands, the second positive system of N_2 ($C^3\prod_u - B^3\prod_g$), and the first negative system of N_2^+ ($B^2\sum_u^+ - X^2\sum_u^+$) were also enhanced obviously. Both electron and vibrational temperature of the plasma jet increased gradually with increasing O_2 concentration in the working medium gas, and first increased and then decreased with increasing axial distance from the plasma jet.

1. Introduction

During flight, an aeroengine faces extremely harsh working conditions due to drastic changes in flight altitude, speed, and attitude, which is a great threat to the safety and stability of the combustion chamber. Therefore, ignition performance is of great importance for aeroengines. With constant increases of flying altitude, speed, and maneuverability of spacecraft instrumentation, it is particularly important to enlarge the ignition boundary of an aeroengine under high altitude, high speed, and other adverse conditions and improve the ability of rapid reignition of the engine after flameout under severe conditions [1–6].

In the past, researchers have focused on the traditional ignition methods, including pilot flame ignition, spark ignition, and hot jet ignition. However, these conventional ignition methods have problems such as small ignition area, low ignition energy, and also narrow ignition boundary and low ignition reliability especially when the engine is operating under harsh conditions. In the past two decades, the plasma ignition technology has become a research hotspot because it has notable characteristics, for example, large ignition energy [7], strong penetration of the flame tongue [8], and high chemical activity [1, 9, 10]. The plasma igniter can improve the ignition reliability and stability of an aeroengine under harsh conditions and can significantly expand its ignition boundary compared with the conventional electric spark igniter [11, 12]. A direct-current (DC) arc plasma igniter exhibits three major mechanisms during ignition, namely, the "high-temperature effect," "chemical effect," and "jet effect." Among these, the "chemical effect" mainly means that the high-temperature arc formed by the plasma igniter ionizes the working medium gas

flowing through the inner cavity of the igniter and generates a plasma containing a large amount of active particles to reduce the activation energy of the chemical reaction, enhance the rate of chemical reaction, and accelerate the progress of the chemical reaction. The "chemical effect" mainly depends on the type of active particles in the plasma jet, which depends, in turn, on the type of gas in the working medium and the discharge parameters [13].

Yamamoto and Tachibana studied the chemical reaction mechanism of CH_4-air mixture ignited by plasma jets of different working media gas through experiments and numerical simulation [14]. The results proved that O and H atoms in plasma jets could significantly promote fuel combustion. However, the plasma igniter used by Yamamoto uses H_2O as the working medium to study the effect of adding different concentrations of Ar or N_2 in H_2O on the ignition delay time.

Zhu and Lopez used a mixture of He and O_2 as the working medium gas to conduct plasma microjet spectral characteristics experiments [15], and the results showed that the higher the concentration of the O_2 component in the mixture, the stronger the emission spectrum of OH and O_3 particles in the plasma jet. Wu et al. obtained a non-equilibrium plasma via the rotating gliding arc discharge method [16] and studied the effect of the working medium gas on the plasma generated by the sliding arc discharge, in which N_2 and air were used separately as working gases for sliding arc discharge. In addition, based on the microwave plasma discharge experiment conducted by Chen and Li using Ar and N_2 as the working gases [17], the effect of gas composition and gas-flow rate on plasma jet temperature was analyzed by emission spectroscopy. Zhu, Wu, and Chen studied a plasma microjet, sliding arc plasma, and microwave plasma, respectively. Compared with a DC arc plasma igniter, these three components have lower ignition energy and ignition reliability. Moreover, the ignition device is too complicated to use directly in ignition systems for aeroengines.

Pei et al. researched the plasma discharge modes under different discharge parameters with N_2 and air as working medium gases for a DC arc plasma igniter [18]. Furthermore, Zhong et al. conducted a high-frequency arc discharge plasma ignition experiment in the combustion chamber of a supersonic ramjet engine [19], in order to study the breakdown characteristics, ignition efficiency, and ablation conditions of the igniter using air and N_2 as the working medium gases. Both Pei and Zhong used a DC arc plasma igniter to study the influence of the working medium gas on the working characteristics of the igniter. However, there are few studies, to the best of our knowledge, in which the effects of working medium gas on the type of active particles and plasma temperature in a DC arc plasma jet have been systematically studied.

To study the influence of different working medium gases on the active particle species and plasma temperature characteristics in a DC arc plasma jet systematically, Ar, N_2, O_2, and N_2-O_2 mixture under different concentrations of the O_2 component were separately adopted as the working medium gas of a plasma igniter. In addition, the optical emission spectroscopy (OES) method was adopted to study the effects of working medium gas and O_2 concentration on emission spectra, active particles, electron temperature, and vibrational temperature of the plasma, which is based on the existing DC arc plasma igniter in the laboratory [20]. Therefore, a foundation is laid for optimizing the design of a DC arc plasma igniter, improving its ignition performance and promoting its application in aeroengines.

2. Experimental Setup and Methods

2.1. Experimental Setup. A schematic of the experimental system is shown in Figure 1, including the plasma igniter, direct-current plasma power supply, gas supply system, voltage probe, oscilloscope, and spectral acquisition system. The concrete structure of the plasma igniter designed in this study was based on that available in the literature [20]; the outer diameter of the igniter was 24 mm, and its length was 180 mm. The input voltage of the DC driving power was 220 V, rated input current was 30 A, rated power was 6 kW, and no-load voltage was 230 V. The gas supply system in the experiment consisted of three high-pressure gas cylinders in parallel, which contained Ar, N_2, and O_2; the gas purity was 99.9%, and the pressure in each cylinder was 10 MPa. The outlet of each gas cylinder was connected separately with a pressure-reducing valve, a flow-regulating valve, a mass flow meter, and a gas check valve; the gas entered into the igniter chamber through the inlet of the plasma igniter, and the gas-flow rate of the working medium was 40–110 g/min. When O_2 was used as the working medium gas of the plasma igniter and the gas flow was 70 g/min, the plasma jet was captured by a Nikon D5200 camera and is shown in Figure 2; the exposure time of the camera was 20 ms. An AvaSpec-ULS2048-4-USB2 four-channel fiber spectrometer (Avantes Co.), with a wavelength in the range of 200–950 nm and a display resolution of 0.1 nm, was selected as the spectral acquisition system. The voltage probe (Tektronix P6015A) can measure the instantaneous high voltage of 20 kV maximally, with a bandwidth of 75 MHz. Moreover, a DPO4104B digital oscilloscope was utilized to record the voltage probe signal, with the largest sample rate of 5 GS/s and a bandwidth of 1 MHz. When measuring the emission spectra of the plasma jet, a fiber-optic probe was fixed at a radial distance of 120 mm from the center line of the igniter. After adjusting the focal length of the fiber-optic probe, the diameter of the spot falling on the center line of the igniter was 2 mm. In addition, when the integral time of the spectrometer was 100 ms, the emission spectra information at axial distances of 10, 15, 20, 25, and 30 mm from the igniter nozzle could be measured.

2.2. Electron Temperature Calculation Method. As an important parameter representing plasma properties, electron temperature directly reflects the average kinetic energy of the electrons in the plasma. At present, electron temperature can basically be calculated, for example, by a double-line method, multispectral line slope method, isoelectronic line method, the Saha–Boltzmann method, and absolute line intensity method [21]. Among these, the double-line method

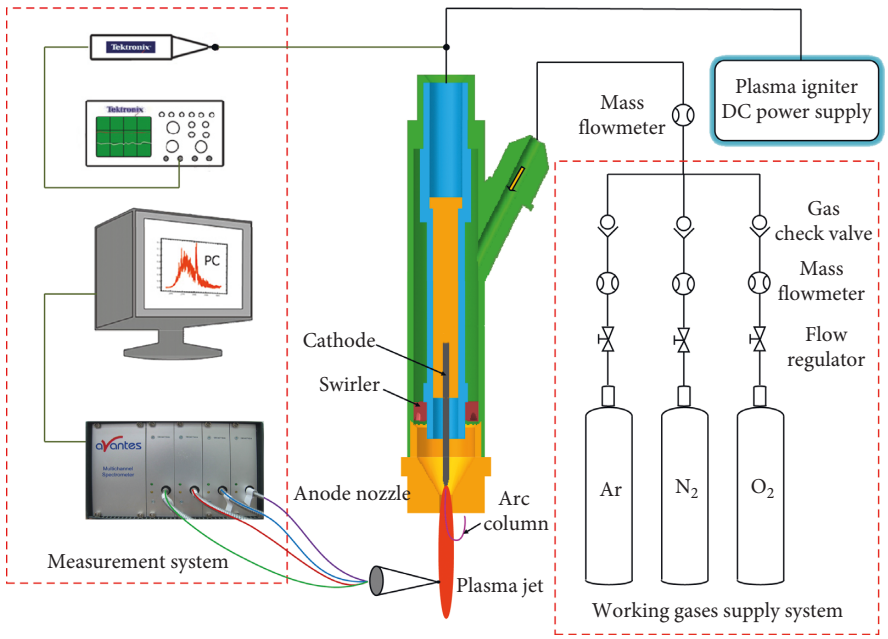

Figure 1: Schematic diagram of the plasma igniter experimental system.

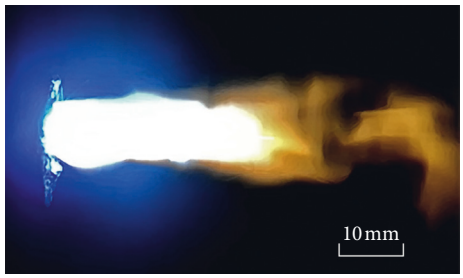

Figure 2: Photos of the O_2 plasma jet.

was adopted in this study to calculate the electron temperature of the plasma jet. When the plasma was in a state of the local thermodynamic equilibrium state, distribution of the electronic energy level bound by the atom satisfied the Boltzmann distribution, and electron velocity met the Maxwell distribution, which can be expressed as follows [22]:

$$\frac{n_m}{n_n} = \frac{g_m}{g_n} \exp\left[\frac{E(m) - E(n)}{kT_e}\right], \quad (1)$$

where T_e denotes electron temperature, n_m and n_n represent the particle number density of m and n energy levels, respectively, g_m and g_n are the respective statistical weights of particles at m and n energy levels, respectively, $E(m)$ and $E(n)$ are the energies of the corresponding energy levels, and k is Boltzmann's constant.

For plasma emission spectra, the spectral intensity of a pair of spectral lines belonging to the same kind of atom can be expressed as follows [21]:

$$I_{mr} = n_m A_{mr} h\nu_{mr},$$
$$I_{nr} = n_n A_{nr} h\nu_{nr}, \quad (2)$$

where I_{mr} and I_{nr} denote the intensities of corresponding spectral lines, ν_{mr} and ν_{nr} the radiation frequencies of electrons transiting from m and n energy levels spontaneously to the r energy level, respectively, A_{mr} and A_{nr} the corresponding transition probabilities, and h is Planck's constant.

The formula for calculating the electron temperature of plasma can be obtained from formulas (1) and (2):

$$T_e = \left|\frac{\Delta E}{\left[k \ln\left(\left(I_{mr}/A_{mr} g_m \lambda_{nr}\right)/\left(I_{nr}/A_{nr} g_n \lambda_{mr}\right)\right)\right]}\right|, \quad (3)$$

where λ_{mr} and λ_{nr} are the respective wavelengths of the corresponding emission spectra.

In terms of DC arc discharge plasma, we consider that the plasma jet was in a local thermodynamic equilibrium state [23]. In view of self-absorption and mutual interference of spectral lines, two representative O I spectral lines (777.54 and 822.18 nm) in the spectra of the plasma jet could be selected to calculate the electron temperature. The spectral parameters are from a table of spectral constants and a handbook of physical constants and are shown in Table 1. After collecting the intensity (I) of two spectral lines in the experiment, the electron temperature of the plasma can be calculated by substituting the spectral intensity (I) into formula (3).

2.3. Vibrational Temperature Calculation Method. The vibrational temperature indicates the intensity of molecular vibration excitation, which can be mainly obtained by the Boltzmann graphic method, spectral intensity contrast method, or spectral line-fitting method [25]. The spectral line intensity of the vibrational band of diatomic molecular emission spectra was [26]

$$I_{v'v''} = hc\nu_{v'v''} p_{v'v''} N_{v'}, \quad (4)$$

where v' and v'' represent the vibrational quantum number of the upper and lower states, respectively, h is Planck's

Table 1: Spectral parameters for calculating electron temperature [24].

Wavelength (nm)	Excited energy (eV)	Statistical weight	Transition probability (s^{-1})
777.54	10.74	3	3.69×10^7
822.18	14.05	7	2.89×10^7

constant ($h = 6.62606975 \times 10^{-34}$ J·s), c is the speed of light ($c = 3 \times 10^8$ m/s), $\nu_{\nu'\nu''}$ is the emission spectral line frequency, $p_{\nu'\nu''}$ is the transition probability between the upper and lower energy levels, and N'_ν denotes the molecular number of the upper state.

The vibrational energy of the upper state ν' of diatomic molecular energy levels can be expressed as follows [27]:

$$E_{\nu'} = \omega_e\left(\nu' + \frac{1}{2}\right) - \omega_e x_e\left(\nu' + \frac{1}{2}\right)^2 + \omega_e y_e\left(\nu' + \frac{1}{2}\right)^3 + \cdots, \tag{5}$$

where the vibrational constant of N_2 is $\omega_e = 4.5586 \times 10^{-5}$ eV, $\omega_e x_e = 3.8259 \times 10^{-7}$ eV, and the third and subsequent terms can be considered negligible [27].

When calculating the vibrational temperature of plasma, the second positive system (SPS) of N_2 was usually adopted [28, 29]. Under the condition of local thermodynamic equilibrium of the DC arc discharge, the particle number distribution of the ν' upper state followed Boltzmann's law [26]:

$$N_{\nu'} = N_0 e^{-E_{\nu'}/kT_\nu}, \tag{6}$$

where T_ν denotes the vibrational temperature.

Equation (7) could be obtained by completing equations (4)–(6) as follows:

$$\ln \frac{I_{\nu'\nu''}}{\nu_{\nu'\nu''} p_{\nu'\nu''}} = C - \frac{E_{\nu'}}{kT_\nu}, \tag{7}$$

where $k = 8.62 \times 10^{-5}$ eV/K and C is a constant.

According to equation (7), it can be seen that $\ln(I_{\nu'\nu''}/\nu_{\nu'\nu''} p_{\nu'\nu''})$ has a linear relationship with $E_{\nu'}$, so the vibrational temperature of the plasma can be calculated based on the slope of this equation. In this study, two vibrational band sequences $\Delta\nu = -2$ (0–2, 1–3, and 2–4) and $\Delta\nu = -3$ (0–3, 1–4, and 2–5) were adopted to conduct linear fitting with the least-squares method when calculating the vibrational temperature, so as to reduce the fitting error. Spectral parameters for calculating the vibrational temperature are shown in Table 2.

3. Results and Discussion

3.1. Spectral Characteristics of Plasma Jets under Diverse Working Medium Gases

3.1.1. Emission Spectra of the Ar Plasma Jet. When the flow rate of Ar was 70 g/min, the output current of the driving power was 20 A, and the axial distance between the fiber-optic probe of the spectrometer and the anode nozzle of the plasma igniter was 10 mm; the plasma jet spectrum in the wavelength range of 650–950 nm is shown in Figure 3.

Table 2: Spectral parameters of the SPS of the nitrogen molecule [30].

$\nu' \longrightarrow \nu''$	Transition wavelength $\lambda_{\nu'\nu''}$ (mm) $\lambda_{\nu'\nu''}$	Transition probability $A_{\nu'\nu''}$ (s^{-1})
$0 \longrightarrow 2$	380.49	2.94×10^6
$1 \longrightarrow 3$	375.54	4.10×10^6
$2 \longrightarrow 4$	371.05	3.37×10^6
$0 \longrightarrow 3$	405.94	0.923×10^6
$1 \longrightarrow 4$	399.84	2.49×10^6
$2 \longrightarrow 5$	394.30	2.63×10^6

As shown in Figure 3, the emission spectra in the Ar plasma jet were mainly concentrated in the range after the wavelength of 690 nm, mainly including the Ar I spectral line (696.54, 706.87, 727.29, 738.40, 751.47, 763.51, 772.42, 794.82, 801.48, 810.37, 811.53, 826.45, 840.82, 842.46, 852.14, 866.79, 912.30, and 922.45 nm) and a small number of weak oxygen lines, such as O I (715.67, 777.54, and 822.18 nm). This means that there were a large number of excited particles of Ar atoms and a small number of excited particles of O atoms existing in the Ar plasma jet. After the Ar was broken down by high voltage in the inner chamber of the igniter, a series of ionization and excitation reactions took place, and a mass of excited-state particles were generated, which were ejected to the outside air from the anode nozzle of the igniter in its anode area under the action of an electric field, magnetic field, and aerodynamic force [31]. Since the ejected plasma jet had fast speed and high temperature, the gas temperature could be above 3000 K [17]; part of the air in the jet region was sucked into the plasma jet, followed by several activated particles containing nitrogen and oxygen produced when N_2 and O_2 in the air were excited.

3.1.2. Emission Spectra of the N_2 Plasma Jet. When the flow rate of N_2 was 70 g/min, the output current of the driving power was 20 A, and the axial distance between the fiber-optic probe of the spectrometer and the anode nozzle of the plasma igniter was 10 mm; the spectrum of the plasma jet in the wavelength range 200–500 nm is shown in Figure 4.

The emission spectra of the N_2 plasma jet were mainly concentrated in the range 200–500 nm. The spectral signal collected after 500 nm was very weak because the activated particles were mainly formed by N_2 ionization, dissociation, and excitation in the chamber of the plasma igniter in the N_2 plasma jet, while the emission spectra of nitrogen-containing active particles were mainly concentrated in the wavelength range 200–500 nm. It can be seen from Figure 4 that the N_2 plasma jet had very complex spectral lines and included a large number of nitrogen-containing atomic lines and molecular and ion band information, indicating that the N_2 plasma jet contained abundant active particles. In the wavelength range 200–300 nm, a nitric oxide β-system NO($B^2\prod - X^2\prod$) and nitric oxide γ-system NO($A^2\sum^+ - X^2\prod$) were found. However, in the wavelength range 300–400 nm, both the metastable atomic lines N I (410.99, 429.32, 447.42, 448.84, 466.05, and 484.74 nm) and N II

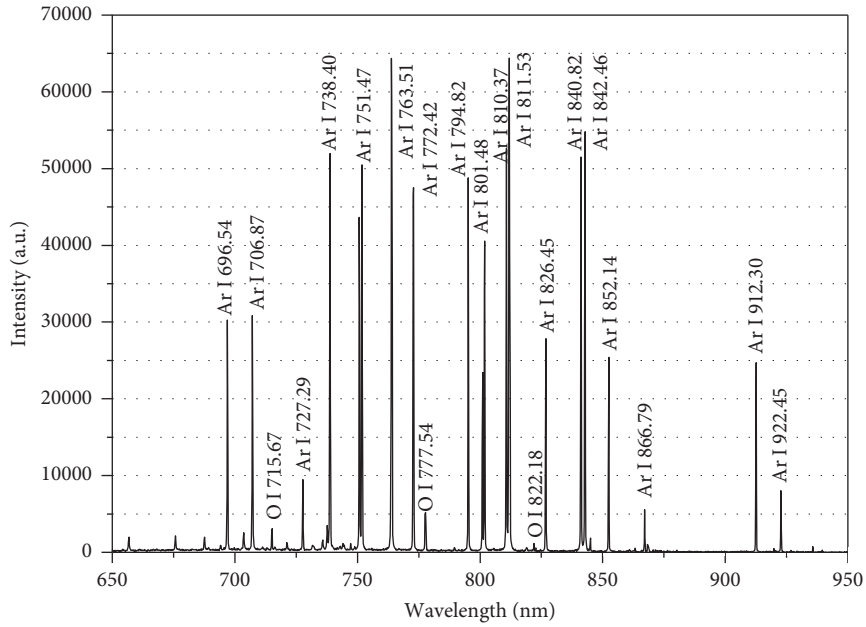

Figure 3: Emission spectra of Ar plasma jet in the wavelength range of 650~950 nm.

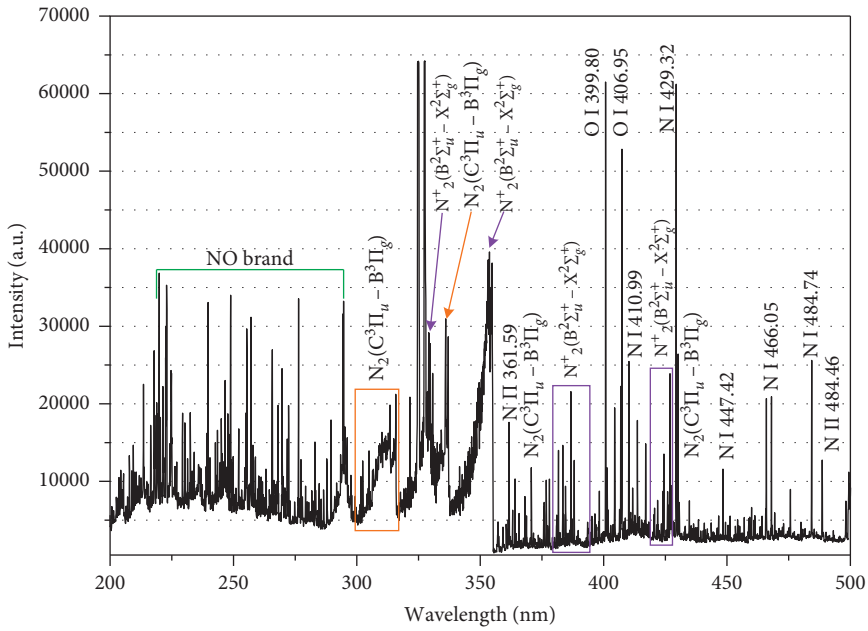

Figure 4: Emission spectra of N_2 plasma jet in the wavelength range of 200–500 nm.

(361.59 and 487.46 nm) formed by the collision of electrons and N_2, and also multiple $N_2(C^3\prod_u - B^3\prod_g)$ second positive systems (SPSs) and $N_2^+(B^2\sum_u^+ - X^2\sum_u^+)$ first negative systems (FNSs) were found. This indicates that not only did excited particles of nitrogen atoms exist, but also a large number of nitrogen-containing molecules and ionic reactive particles existed, such as $NO(A^2\sum^+)$, $NO(B^2\prod)$, $NO(X^2\prod)$, $N_2(C^3\prod_u)$, $N_2(B^3\prod_g)$, $N_2^+(B^2\sum_u^+)$, and $N_2^+(X^2\sum_u^+)$ [32]. Meanwhile, metastable emission spectra of O, consisting of O I (399.80 and 406.95 nm), were found in the N_2 plasma jet because the mixing of the plasma jet with the surrounding air dissociates and excites the O_2 in the air, and then active particles with O excited states were generated due to high temperature.

3.1.3. Effect of O_2 Concentration on Emission Spectra of the Plasma Jet. N_2-O_2 mixture with different O_2 components was used as the working medium gas of the plasma igniter in this study to investigate the influence of O_2 concentration on active particles and emission spectra of the plasma jet. When the flow rate was 70 g/min and the axial distance between the fiber-optic probe of the spectrometer and the anode nozzle of the plasma igniter was still 10 mm, the spectral image of the plasma jet is shown in Figure 5.

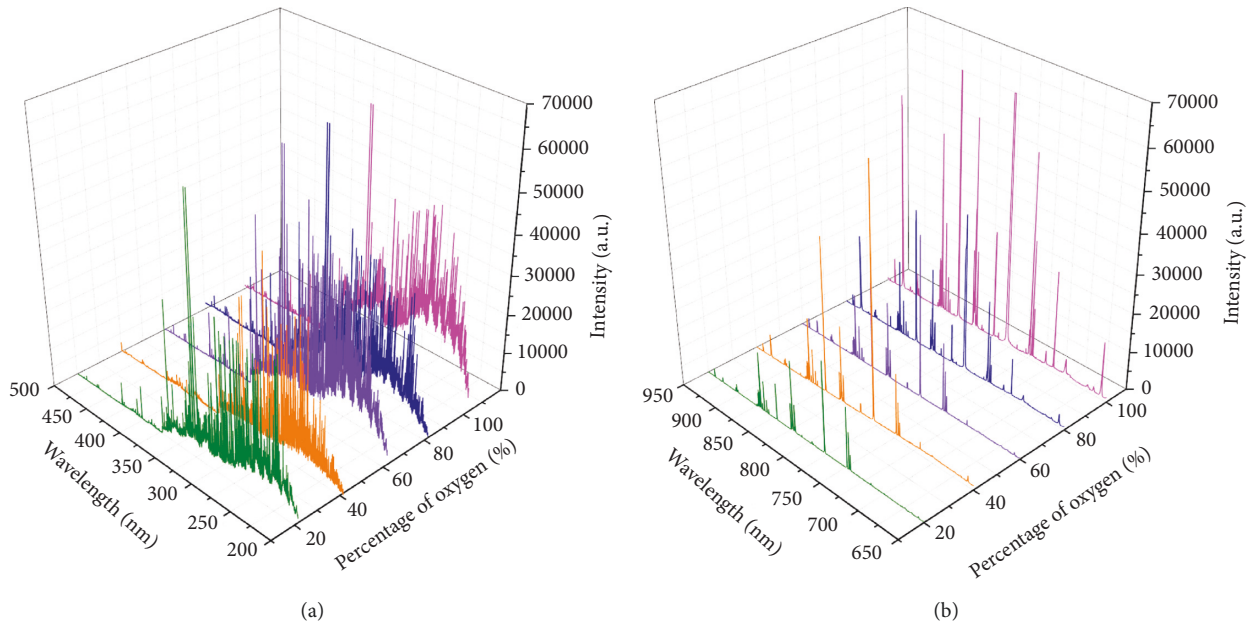

Figure 5: Spectral images of the plasma jet under different O_2 components. (a) Spectral images in the wavelength range of 200–500 nm. (b) Spectral images in the wavelength range of 650–950 nm.

According to Figure 5, in the gas mixture of 20% O_2, the emission spectrum of the plasma jet was mainly concentrated in the wavelength range 200–360 nm. According to the analysis in the preceding section, the wavelength range mainly included nitric oxide β-system NO ($B^2\prod - X^2\prod$), nitric oxide γ-system NO ($A^2\sum^+ - X^2\prod$), N_2 ($C^3\prod_u - B^3\prod_g$) (SPS), and N_2^+ ($B^2\sum_u^+ - X^2\sum_u^+$) (FNS). However, only a few weak spectral lines could be observed in the wavelength range 650–950 nm, namely, O I (777.54 and 822.18 nm) and O II (868.61 nm), through searching the National Institute of Standards and Technology (U.S.) spectral database [24]. In addition, it was found that the spectral intensity in the wavelength range 650–950 nm in emission spectra of the plasma jet increased gradually with increasing O_2 concentration because, in the working gas with the same flow rate, if the O_2 concentration was higher, the O_2 concentration involved in the reaction would be higher, and the concentration of oxygen-containing active particles would be higher. However, Figure 5(a) indicates that the spectral intensity of NO bands, the second positive system of N_2 ($C^3\prod_u - B^3\prod_g$) (SPS) and the first negative system of N_2^+ ($B^2\sum_u^+ - X^2\sum_u^+$) (FNS) within the wavelength range 200–360 nm would increase along with increasing O_2 concentration in the working medium gas. This shows that, as the concentration of O_2 in the working medium gas increased, the concentration of nitrogen-containing active particles in the plasma jet also increased. To explain why the nitrogen-containing active particles in the plasma jet increased with increasing O_2 concentration in the working medium gas, the arc voltage waveform between the cathode and anode of the igniter was analyzed when the plasma igniter operated stably. Under different O_2 concentrations, the arc voltage waveform is shown in Figure 6 and the mean arc voltage in Figure 7.

It can be seen from Figures 6 and 7 that the mean value, standard deviation, and fluctuation of arc voltage increased with increasing O_2 concentration in the working medium gas. Zhang et al. found by experiment that arc pulsation would have an effect on arc voltage [20], and if the arc was longer, the arc voltage would be higher. Trelles et al. divided the arc motion of a DC plasma into three modes [33]: (1) steady mode, in which the arc voltage had very small fluctuation, and the root of arc basically stayed in one place; (2) takeover mode, in which the voltage fluctuated in small amplitude, and the voltage changed in periodicity; and (3) restrike mode, in which the arc voltage had relatively large fluctuation, and the arc exhibited an obvious large-scale shunt phenomenon at this time. It can also be noted from Figures 6 and 7 that the voltage fluctuation was small, and the arc was stable when the O_2 concentration was 20%. The arc operated in the steady mode at this moment, and the plasma ejected from the anode nozzle of the igniter entered the air in a stable form. With increasing O_2 concentration in the working medium gas, the fluctuation range of the arc voltage became obviously large, presenting typical restrike mode. The arc started moving at the igniter nozzle, and the arc shunt phenomenon also increased gradually. Meanwhile, the plasma jet showed an obvious pulsating state under the influence of arc motion, which resulted in the increase of the entrainment effect of the plasma jet on the surrounding air, and then a large amount of surrounding air reacted with high-temperature plasma jet under the action of entrainment. The increasing O_2 concentration in the working medium gas enlarged both the pulsating state and entrainment effect of the plasma jet, and then more N_2 in the air was involved in the reaction, producing nitrogen-containing active particles. Therefore, the intensity of NO molecular bands, the SPS,

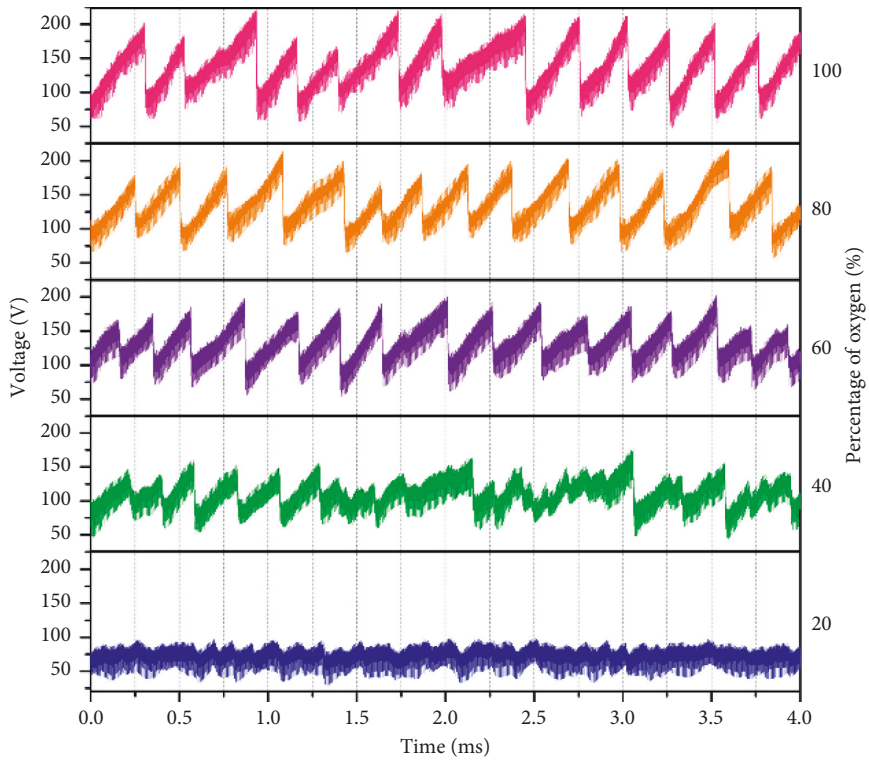

Figure 6: Arc voltage waveform of the plasma igniter under different O_2 concentrations.

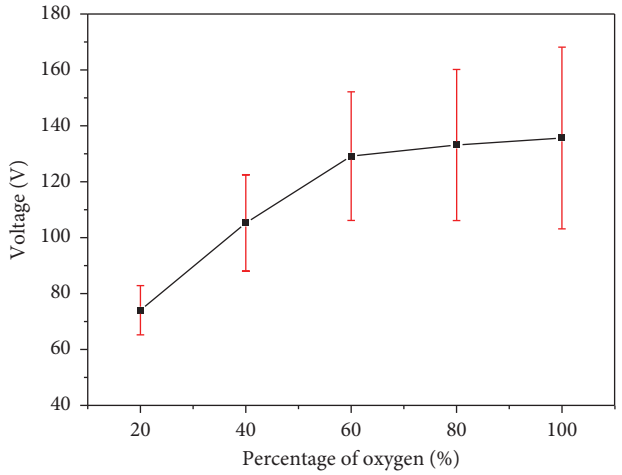

Figure 7: Mean arc voltage of the plasma igniter under different O_2 concentrations. The error bars represented the standard deviation of arc voltage from 0 ms to 4 ms presented in Figure 6.

and the FNS also increased with increasing O_2 concentration in the working medium gas.

3.2. Temperature Characteristics of the Plasma Igniter in Different Working Medium Gases

3.2.1. Effects of Working Medium Gases on Electron Temperature of the Plasma Jet. Ar, N_2, O_2, and N_2-O_2 mixture of different O_2 components were separately used as the working medium gases of the plasma igniter to study the influence of the working-medium-gas type and O_2 concentration on the electron temperature of the plasma jet. The gas-flow rate was 70 g/min, the emission spectra at axial distances of 10, 15, 20, 25, and 30 mm from the anode nozzle of the igniter were measured separately, and the electron temperature spatial distribution of the plasma jet was also calculated, as shown in Figure 8.

It can be seen from Figure 8 that the electron temperature of the O_2 plasma jet was the highest and could reach up to 4.2 eV. However, when Ar or N_2 was used as the working medium gas, the electron temperature of the plasma jet was relatively low, which was basically maintained at approximately 1.0 eV. It can also be observed that the electron temperature of the plasma jet increased along with increasing O_2 concentration in the working medium gas. This indicated that the higher the O_2 concentration in the working gas, the higher the electron energy in the plasma jet, which could violently collide with a large number of molecules in the working medium gas to generate more active particles. However, when Ar or N_2 was used as the working medium gas of the plasma igniter, the electrons in the plasma jet had lower energy and could not excite the particles to transit between the high-energy states and generate more active particles.

Figure 8 also shows that when O_2 was used as the working medium gas, the electron temperature of the plasma jet first increased and then decreased in the axial direction, and the maximum value was reported when the axial distance was 25 mm. However, when Ar or N_2 was used as the working medium gas, the electron temperature of the plasma jet also first increased and then decreased, while the maximum value occurred approximately 15 mm

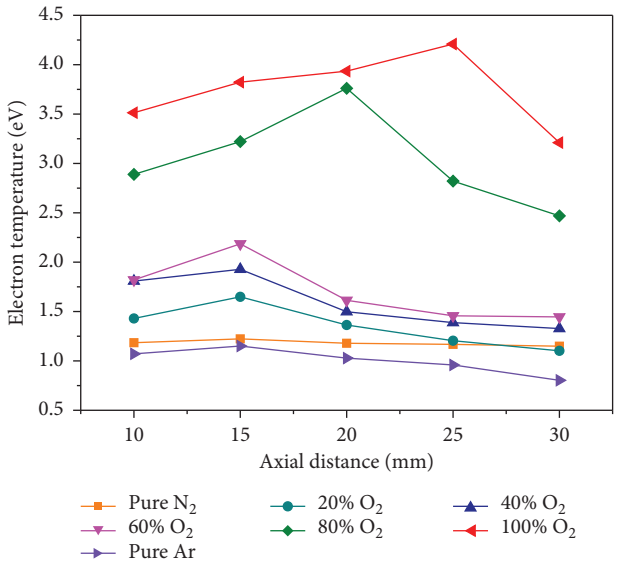

Figure 8: Axial spatial distribution of the electron temperature of the plasma jet.

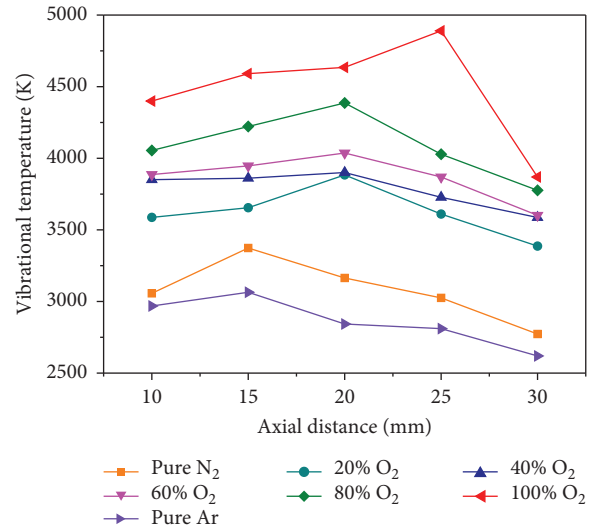

Figure 9: Axial spatial distribution of vibrational temperature of the plasma jet.

from the anode nozzle. This was because the length of the arc column and plasma jet formed at the anode nozzle of the igniter was different when different gases were used as the working medium gas of the igniter. Specifically, when O_2 was used as the working medium gas, the arc column formed at the anode nozzle of the igniter was relatively long, and the high-temperature arc continuously provided energy for heating the working medium in order to promote the generation of active particles. However, when Ar or N_2 was used as the working medium gas, the arc column formed was relatively short. When the axial distance was greater than 15 mm, the electron energy of the plasma jet decreased continuously since the plasma jet was far from the high-temperature arc.

3.2.2. Effects of Working Medium Gases on Vibrational Temperature of the Plasma Jet. Ar, N_2, O_2, and N_2-O_2 mixture of different O_2 components were used as the working medium gas of the plasma igniter separately to study the influence of the working-medium-gas type and O_2 concentration on the vibrational temperature of the plasma jet. According to the results of the previous analysis, it was found that, when Ar or O_2 was used as the working gas of the igniter, high-speed plasma jets would entrain the air from the environment, and the plasma jet also included spectral bands of the SPS of N_2, so the SPS of N_2 can still be used to calculate the vibrational temperature of the plasma jet. The gas-flow rate was 70 g/min, the emission spectra at axial distances of 10, 15, 20, 25, and 30 mm from the anode nozzle of the igniter were measured separately, and the vibrational temperature spatial distribution of the plasma jet was also calculated, as shown in Figure 9.

It can be observed from Figure 9 that the vibrational temperature had the same tendency in the axial direction of the plasma jet when different working medium gases were used as the working medium of the plasma igniter, which first increased and then decreased, while the location of the maximum vibrational temperature was different. When Ar or N_2 was used as the working medium gas, the maximum vibrational temperature occurred in the position that was approximately 15 mm from the anode nozzle; meanwhile, the maximum vibrational temperature occurred increasingly farther away from the igniter nozzle along with increasing O_2 concentration in the working medium gas. Moreover, when O_2 was used as the working medium gas of the igniter, the maximum vibrational temperature occurred in the position that was 25 mm from the anode nozzle, which could reach up to 4890 K. However, the vibrational temperature of the Ar plasma jet at this position was only 2810 K. It can also be seen from Figure 9 that the vibrational temperature of the plasma jet constantly improved with increasing O_2 concentration in the working medium gas, indicating that the vibrational excitation intensity of molecules in the plasma jet increased with increasing O_2 concentration in the working medium gas.

4. Conclusions

In this study, to study the effects of different working medium gases on the type of active particles and plasma temperature characteristics in DC arc plasma jets systematically, Ar, N_2, O_2, and N_2-O_2 mixture of different O_2 components were separately used as the working medium gas of a plasma igniter, and the emission spectra of the plasma jet were measured by a spectrometer to obtain the influence rules of different working medium gases and O_2 concentrations on the emission spectra of the plasma jet and active particles. In addition, the effects of gas type and O_2 concentration of the working medium gas on both electron and vibrational temperature of the plasma jet and the spatial distribution of electron and vibrational temperature in the axial direction of the plasma jet were obtained through analysis and calculation, which lays the foundation for promoting the application of plasma igniters in aeroengines.

The main conclusions are the following:

(1) The emission spectra of the Ar plasma jet were mainly concentrated in the wavelength range 690–920 nm, mainly including Ar I spectral lines and weaker oxygen lines. In addition, the active particles in the Ar plasma jet were mainly metastable particles in the excited state of Ar.

(2) When N_2 was used as the working medium gas of the plasma igniter, the emission spectra were mainly concentrated at 200–500 nm, and the atomic spectral lines coexisted with molecular and ion bands, the metastable atomic spectral lines of which were mainly N I and N II. Meanwhile, there were few oxygen-containing O I atomic lines. The band of molecules and ions in a spectrum included a large number of nitric oxide β-system, nitric oxide γ-system, and numerous SPSs and FNSs of nitrogen molecules or ions. Moreover, the active particles included in the N_2 plasma jet mainly included nitrogen-containing molecules and ions, such as $NO(A^2\sum^+)$, $NO(B^2\prod)$, $NO(X^2\prod)$, $N_2(C^3\prod_u)$, $N_2(B^3\prod_g)$, $N_2^+(B^2\sum_u^+)$, and $N_2^+(X^2\sum_u^+)$, as well as metastable active particles of N and O atoms.

(3) With increasing O_2 concentration in the working medium gas, the spectral line intensity of oxygen-containing particles in the plasma jet was obviously enhanced, the pulsation of arc voltage increased, and the turbulence pulsation of plasma jet increased, so more surrounding air was entrained into the reaction. Therefore, with increasing O_2 concentration in the working medium gas, the spectral intensities of nitrogen-containing atomic spectral lines, NO molecular bands, SPSs, and FNSs in emission spectra were significantly enhanced.

(4) When O_2 was used as the working medium gas, the electron temperature of the plasma jet was the highest, and the electron temperature at approximately 25 mm axial from the anode nozzle of the igniter was 4.2 eV. However, when Ar or N_2 was used as the working medium gas, the electron temperature of the plasma jet was relatively low, basically around 1.0 eV. O_2 concentration had a great influence on the electron temperature, which increased with increasing O_2 concentration; the electron temperature first increased and then decreased with increasing axial distance of the plasma jet.

(5) When O_2 was used as the working medium gas, the vibrational temperature of the plasma jet was the highest; the vibrational temperature at approximately 25 mm axial from the anode nozzle of the igniter was 4889.6 K, while the vibrational temperature of the Ar plasma jet was the lowest. The vibrational temperature increased with increasing O_2 concentration. In addition, the vibrational temperature first increased and then decreased with increasing axial distance of the plasma jet.

Furthermore, our results suggest that the plasma igniter with oxygen medium gas will have the best ignition performance on the aeroengines. However, the ignition process of the aeroengines is affected by many factors. In order to verify that the plasma igniter with oxygen has the best ignition performance, we will carry out the experimental research on the ignition process of the plasma igniter with different working medium gases in the real combustion chamber in the future.

Data Availability

The data used to support the findings of this study have not been made available because the experimental data involved in the paper are all obtained based on our own designed experiments and need to be kept confidential.

Conflicts of Interest

The authors declare that there are no conflicts of interest regarding the publication of this paper.

Acknowledgments

This work was supported by the National Natural Science Foundation of China under project nos. 51436008 and 51806245.

References

[1] Y. Ju and W. Sun, "Plasma assisted combustion: dynamics and chemistry," *Progress in Energy and Combustion Science*, vol. 48, pp. 21–83, 2015.

[2] Z. C. Zhao, L. M. He, H. L. Zhang et al., "Experimental study on working characteristics of direct current plasma jet igniter," *Plasma Research Express*, vol. 1, no. 2, article 025015, 2019.

[3] E. Mastorakos, "Forced ignition of turbulent spray flames," *Proceedings of the Combustion Institute*, vol. 36, no. 2, pp. 2367–2383, 2017.

[4] S. M. Starikovskaia, "Plasma assisted ignition and combustion," *Journal of Physics D: Applied Physics*, vol. 39, no. 16, pp. 265–299, 2006.

[5] S. Huang, Y. Wu, H. Song et al., "Experimental investigation of multichannel plasma igniter in a supersonic model combustor," *Experimental Thermal and Fluid Science*, vol. 99, pp. 315–323, 2018.

[6] A. Starikovskiy and N. Aleksandrov, "Plasma-assisted ignition and combustion," *Progress in Energy and Combustion Science*, vol. 39, no. 1, pp. 61–110, 2013.

[7] A. Y. Starikovskii, N. B. Anikin, I. N. Kosarev et al., "Nanosecond-pulsed discharges for plasma-assisted combustion and aerodynamics," *Journal of Propulsion and Power*, vol. 24, no. 6, pp. 1182–1197, 2008.

[8] Y. Guan, G. Zhao, and X. Xiao, "Design and experiments of plasma jet igniter for aeroengine," *Propulsion and Power Research*, vol. 2, no. 3, pp. 188–193, 2013.

[9] A. A. Tropina, M. N. Shneider, and R. B. Miles, "Ignition by short duration, nonequilibrium plasma: basic concepts and applications in internal combustion engines," *Combustion Science and Technology*, vol. 188, no. 6, pp. 831–852, 2015.

[10] D. Singleton, S. J. Pendleton, and M. A. Gundersen, "The role of non-thermal transient plasma for enhanced flame ignition in C_2H_4–air," *Journal of Physics D: Applied Physics*, vol. 44, no. 2, article 022001, 2011.

[11] W. T. Sun, *Non-Equilibrium Plasma-Assisted Combustion*, Princeton University, Princeton, NJ, USA, 2013.

[12] K. V. Khodataev, "Microwave discharges and possible applications in aerospace technologies," *Journal of Propulsion and Power*, vol. 24, no. 5, pp. 962–972, 2008.

[13] F. Li, X.-L. Yu, Y.-G. Tong et al., "Plasma-assisted ignition for a kerosene fueled scramjet at Mach 1.8," *Aerospace Science and Technology*, vol. 28, no. 1, pp. 72–78, 2013.

[14] Y. Yamamoto and T. Tachibana, "Feasibility study of water plasma jets for combustion promotion," *Fuel*, vol. 186, pp. 846–852, 2016.

[15] W. D. Zhu and J. L. Lopez, "A dc non-thermal atmospheric-pressure plasma microjet," *Plasma Sources Science and Technology*, vol. 21, no. 3, article 034018, 2012.

[16] A. J. Wu, H. Zhang, X. D. Li, S. Y. Lu, C. M. Du, and J. H. Yan, "Spectroscopic diagnostics of rotating gliding arc plasma codriven by a magnetic field and tangential flow," *IEEE Transactions on Plasma Science*, vol. 42, no. 11, pp. 3560–3568, 2014.

[17] C. J. Chen and S. Z. Li, "Spectroscopic measurement of plasma gas temperature of the atmospheric-pressure microwave induced nitrogen plasma torch," *Plasma Sources Science and Technology*, vol. 24, no. 3, article 035017, 2015.

[18] X. K. Pei, J. Kredl, X. P. Lu et al., "Discharge modes of atmospheric pressure DC plasma jets operated with air or nitrogen," *Journal of Physics D: Applied Physics*, vol. 51, no. 38, article 384001, 2018.

[19] W. Zhong, W. Xi, L. Duan, Q. Xu, and Q. Li, "Experimental investigation on the plasma torch used for scramjet ignition enhancement," *Journal of Applied Mathematics and Physics*, vol. 3, no. 8, pp. 956–964, 2015.

[20] H.-L. Zhang, L.-M. He, G.-C. Chen, W.-T. Qi, and J.-L. Yu, "Experimental study on ignition characteristics of kerosene-air mixtures in V-shaped burner with DC plasma jet igniter," *Aerospace Science and Technology*, vol. 74, pp. 56–62, 2018.

[21] R. Wu, Y. Li, S. G. Zhu et al., "Emission spectroscopy diagnostics of plasma electron temperature," *Spectroscopy and Spectral Analysis*, vol. 28, no. 4, p. 735, 2008.

[22] B. Y. Man, "Particle velocity, electron temperature, and density profiles of pulsed laser-induced plasmas in air at different ambient pressures," *Applied Physics B: Lasers and Optics*, vol. 67, no. 2, pp. 241–245, 1998.

[23] Z. Duan and J. Heberlein, "Arc instabilities in a plasma spray torch," *Journal of Thermal Spray Technology*, vol. 11, no. 1, pp. 44–51, 2002.

[24] A. Kramida, Y. Ralchenko, J. Reader, and NIST ASD Team, *NIST Atomic Spectra Database (Version 5.6.1)*, National Institute of Standards and Technology, Gaithersburg, MD, USA, 2018.

[25] U. Kogelschatz, "Filamentary, patterned, and diffuse barrier discharges," *IEEE Transactions on Plasma Science*, vol. 30, no. 4, pp. 1400–1408, 2002.

[26] P. C. Zheng, H. M. Wang, J. Q. Li et al., "Characterization of an atmospheric pressure DC microplasma jet," *Spectroscopy and Spectral Analysis*, vol. 29, no. 2, pp. 289–292, 2009.

[27] J. Y. Chen, L. F. Dong, Y. Y. Li et al., "Plasma parameters of square superlattice pattern in a dielectric barrier discharge," *Acta Physica Sinica*, vol. 61, no. 7, article 075211, 2012.

[28] E. M. Hollmann and A. Y. Pigarov, "Measurement and modeling of molecular ion concentrations in a hydrogen reflex-arc discharge," *Physics of Plasmas*, vol. 9, no. 10, pp. 4330–4339, 2002.

[29] N. Masoud, K. Martus, M. Figus, and K. Becker, "Rotational and vibrational temperature measurements in a high-pressure cylindrical dielectric barrier discharge (C-DBD)," *Contributions to Plasma Physics*, vol. 45, no. 1, pp. 32–39, 2005.

[30] D. E. Shemansky and A. L. Broadfoot, "Excitation of N_2 and N_2^+ systems by electrons—I. Absolute transition probabilities," *Journal of Quantitative Spectroscopy and Radiative Transfer*, vol. 11, no. 10, pp. 1385–1400, 1971.

[31] C. K. Wu and W. X. Pan, "Unsteadiness in non-transferred dc arc plasma generators," *Theoretical and Applied Mechanics Letters*, vol. 1, no. 2, article 024001, 2011.

[32] Y. Akishev, M. Grushin, V. Karalnik, A. Petryakov, and N. Trushkin, "Non-equilibrium constricted dc glow discharge in N_2 flow at atmospheric pressure: stable and unstable regimes," *Journal of Physics D: Applied Physics*, vol. 43, no. 7, article 075202, 2010.

[33] J. P. Trelles, E. Pfender, and J. Heberlein, "Multiscale finite element modeling of arc dynamics in a DC plasma torch," *Plasma Chemistry and Plasma Processing*, vol. 26, no. 6, pp. 557–575, 2006.